Microscopic description of the current–voltage characteristics of a bulk-heterojunction organic solar cell under illumination

Osamu Takeuchi[1], Noriaki Takeuchi[1†], Takahiro Ochiai[1,2], Hirokazu Kato[1], Shoji Yoshida[1], and Hidemi Shigekawa[1]
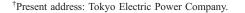
[1]*Faculty of Pure and Applied Sciences, University of Tsukuba, Tsukuba, Ibaraki 305-8573, Japan*
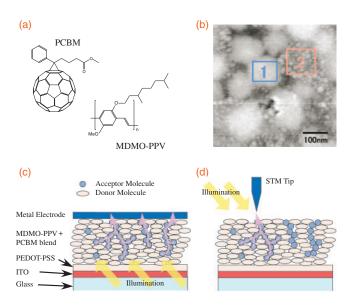[2]*TAKANO Co., Ltd., Miyada, Nagano 399-4301, Japan*

Measurement of the local current–voltage (J–V) characteristics of a MDMO-PPV:PCBM bulk-heterojunction (BHJ) solar cell by using light-modulated scanning tunneling spectroscopy (LM-STS) revealed that the open-circuit voltage (V_{OC}) differs from one region to another. Consequently, when the bias voltage is set near V_{OC}, the generated photocurrent in some regions is internally lost in other regions through leakage. In the same manner, the external J–V characteristics of a BHJ solar cell device results from numerous parallely connected local solar cells. LM-STS allows us to interpret the external J–V characteristics of a device in terms of the characteristics of the local solar cells. © 2014 The Japan Society of Applied Physics

Organic solar cells have attracted considerable interest from scientists because they are predicted to be cost efficient, resource saving, lightweight, and mechanically flexible.[1–7] Compared to conventional crystalline Si solar cells, they have many more inhomogeneous structures. Thus, to improve their generation efficiency and lifetime, it is important to understand their external characteristics from a microscopic viewpoint. For instance, in the equivalent circuit model of a conventional solar cell, a current source, which generates photocurrent under illumination, is connected in parallel to an internal diode and a leakage resistor as well as to an output resistor in series. When no external circuit is connected, the generated photocurrent increases the device voltage until the leakage current through the internal diode and resistor balances the generation. In more sophisticated models, additional components are introduced to account for the deviation of the experimentally observed characteristics from the simplest model.[8–12] As has been suggested in many studies,[13–17] however, the microscopic characteristics of an organic solar cell vary from one region to another within the device. Thus, if one takes this inhomogeneity into account, the equivalent circuit model should be much more complex. In such a model, numerous small solar cells, the characteristics of which slightly differ from each other, are all connected in parallel. To obtain such a microscopic view of an organic solar cell, in this study, we investigated the local characteristics of a bulk-heterojunction (BHJ) type solar cell[18–20] by applying scanning tunneling microscopy (STM) and light-modulated scanning tunneling spectroscopy (LM-STS).[21,22] The generation of photocurrent and the internal leakage of the generated current are discussed in terms of the local current–voltage (J–V) characteristics under illumination.
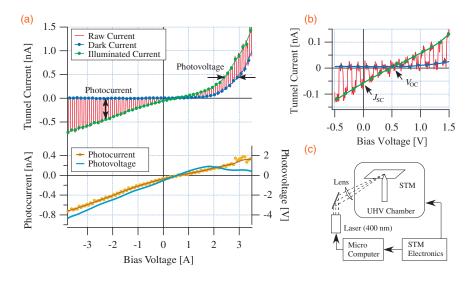
The sample was based on a soluble fullerene derivative 1-(3-methoxycarbonyl)propyl-1-phenyl[6,6]C61 (PCBM) as an electron acceptor and poly[2-methoxy-5-(3′,7′-dimethyl-octyloxy)-1,4-phenylenevinylene] (MDMO-PPV) as a donor, which was prepared as follows. First, as a hole transport layer, PEDOT-PSS[23] was spin-coated on an indium tin oxide (ITO) thin film on a glass substrate (TOYOBO 300R) and annealed at 140 °C in air for 10 min. Then, a toluene solution of an MDMO-PPV:PCBM mixture [Fig. 1(a)] at a concentration of 3 mg/mL was spin-coated in a dry-nitrogen environment to form the BHJ active layer. STM and STS

Fig. 1. Schematics of the sample structure. (a) PCBM and MDMO-PPV molecules. (b) STM topography measured on the MDMO-PPV:PCBM blend layer. (c) Ordinary BHJ organic solar cell setup. (d) BHJ organic solar cell in the present study.

measurements (Omicron VT-STM) were performed at room temperature in an ultrahigh-vacuum (UHV) condition by using an electrochemically etched tungsten tip that was annealed by electron bombardment in an ultrahigh vacuum for oxide removal. An STM image of the topography of the above-noted sample under illumination is shown in Fig. 1(b). In agreement with the literature,[13,14] the PCBM-rich domains with circular or elliptical shapes were self-organized in the MDMO-PPV-rich matrix. The lateral diameters of the PCBM-rich domains ranged from 50 to 150 nm, and one of them is indicated by the boxed "1" in the figure. In contrast, in the MDMO-PPV-rich matrix area, small clusters with diameters of a few tens of nanometers are imaged, as seen in the boxed area marked "2". Compared to the ordinary solar cell structure shown in Fig. 1(c), in this setup, the planer metal electrode that gathers electrons from the solar cell is replaced by the STM tip, as shown in Fig. 1(d). Thus, the STM tip only gathers the locally generated electrons beneath the tip via the tunnel junction. Another difference is that the illumination is from the side of the STM tip in the present study, whereas it is from the side of the transparent substrate in the ordinary solar cell setup.
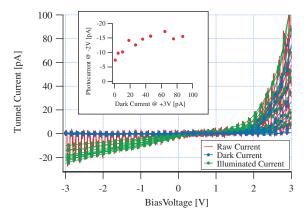
†Present address: Tokyo Electric Power Company.

Fig. 2. Typical LM-STS result and setup. (a) Raw J–V curve in chopped illumination and calculated curves from the raw curve. (b) Magnified plot of (a). (c) LM-STS setup. The solar cell sample is intermittently illuminated synchronously to STM and STS measurement.

For LM-STS measurement, the sample was illuminated by a violet laser ($\lambda = 400$ nm) of ~5 mW, which was electrically chopped synchronously with the STM scan under the control of a microcomputer, as illustrated in Fig. 2(c). The laser beam is focused to a diameter of a few tens of micrometers on the sample surface. A typical LM-STS result is shown in Fig. 2(a). During the J–V curve measurements with a bias sweep velocity of 8 V/s, the laser illumination is chopped at 100 Hz. Thus, as seen in the magnified plot in Fig. 2(b), the raw J–V curves (shown in red) oscillate with large amplitudes. To retrieve the current values under illuminated and dark conditions, the tunnel current in each dark and illuminated half-period is averaged, excluding the transient regions (10% of the period). The averaged values are indicated by the blue (dark) and green (illuminated) markers. By smoothly tracing these points, dark and illuminated local J–V curves can be simultaneously obtained from one raw J–V curve. Once the two curves are obtained, the photoinduced current (photocurrent) and the photovoltage can be obtained from the vertical and horizontal separation of the two curves, as illustrated in Fig. 2(a).

When measured on a solar cell, the dark J–V curves exhibit rectifying characteristics [the blue curve in Fig. 2(a)] because of the existence of the p–n junction in the sample. Almost negligible current flows when a negative sample bias voltage, i.e., a backward bias voltage, is applied, whereas the current increases rapidly as the positive bias voltage, i.e., the forward bias voltage, increases. Under illumination, finite current flows at zero bias voltage, as shown in Fig. 2(b). This current is referred to as the short-circuit current (J_{SC}). The photocurrent decreases when a forward bias voltage is applied. The bias voltage at which the photocurrent becomes zero is called the open-circuit voltage (V_{OC}). In between these two points, the current under illumination flows against the bias voltage; i.e., this region is the solar cell's working condition.

In an LM-STS measurement, local regions of the solar cell are biased via a tunnel junction. Thus, if the tunnel conductance is smaller than that of the solar cell, the observed current is determined mainly by the tunnel conductance rather than by the properties of the solar cell. To ensure that the tunnel conductance is large enough for measurement, we

Fig. 3. Dependence of LM-STS result on tip–sample distance measured on a PCBM-rich cluster. The inset shows the dependence on the tunnel conductance under the dark condition.

placed the STM tip on a PCBM-rich cluster and conducted LM-STS measurements with varying tip–sample distances.

The result is shown in Fig. 3. Reflecting the variation of tip–sample distance, the dark and illuminated current under positive bias voltage varied by as much as dozens of times, whereas the illuminated current under negative bias voltage does not change as much. Under positive bias voltage, the p–n junction between MDMO-PPV and PCBM is forwardly biased. Thus, the tunnel conductance becomes relatively small and governs the total conductance. In contrast, under negative bias voltage, no dark current is observed because of the reversely biased p–n junction. When illuminated, photo-generated carriers are collected by the STM tip and a finite current flows. Thus, this condition is called the photoamperic regime.[24] When the internal resistance of the solar cell and the tunnel resistance are both small, a small bias voltage is needed to collect most of the generated electrons by using the STM tip. Thus, the photocurrent saturates at small bias voltage. When the internal resistance is large, the voltage drop at the resistance limits the current. Thus, the photocurrent increases linearly with the bias voltage. The linear dependence of the photocurrent illustrated in Fig. 3 corresponds to this situation.
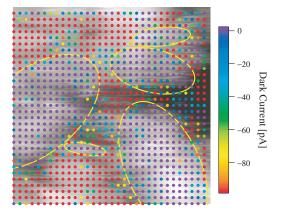
Fig. 4. Dark-current distribution with a sample bias of -3.5 V overlapped on an STM topographic image measuring 500×500 nm^2 with a feedback condition of 4 V and 1.5 nA. The yellow ellipses are drawn arbitrarily to guide the eye.

If tunnel resistance is not negligible, the gradient of the photocurrent will be further decreased depending on the tip–sample distance. Because the negatively biased region against V_{OC} is the working condition of the solar cells, it is favorable to have tunnel resistance be negligible in this region. To find the condition, the photocurrent at -2 V is plotted against the dark current at $+3$ V in the inset of Fig. 3. One can see that the photoconductance depends on the tunnel conductance only when the dark current at $+3$ V is smaller than 30 pA. Hereafter, we choose the tunnel condition so that a dark current of $\sim$500 pA flows at $+3$ V to maintain negligible tunnel resistance.

As shown in Fig. 4, 1024 J–V curves at 32×32 grid points were measured during the measurement of an STM topographic image with an area of 500×500 nm^2. The curve shown in Fig. 2(a) was measured in the middle of the lower-right yellow ellipse. For the LM-STS measurement, the tip–sample distance was regulated by a feedback condition of 4 V and 1.5 nA in the dark condition. In Fig. 4, some elliptical regions (which are indicated by the yellow ellipses) can be

distinguished in the dark-current distribution. The colored grid points in Fig. 4 show the dark current at -3.5 V. As discussed above, when the tip is on the PCBM-rich domains, almost no current flows owing to the rectification by the p–n junction at the MDMO-PPV:PCBM interface. When the tip is on the MDMO-PPV-rich matrix, the Schottky barrier possibly generated between the tip and the sample can also exhibit rectification in the same direction. In the present case, however, the barrier is not thick enough to prevent electron tunneling through the barrier. As a result, finite current is observed when the tip is not on the elliptic PCBM-rich domains.

Figure 5 shows the photocurrent distribution as a function of the sample bias voltage in the same area shown in Fig. 4. Figure 5(a) corresponds to the J_{SC} mapping. As expected, the regions with large J_{SC} roughly coincide with the yellow elliptical regions, where the clear rectification characteristic was observed. Upon closer inspection, however, one observes that some parts in the yellow ellipses do not exhibit as large a J_{SC} value as other parts. We interpret this as due to higher internal resistance in such regions. This point will be discussed in a future publication. The lower part of the lower-right cluster and the upper part of the middle-left cluster exhibited the largest J_{SC}. Though the magnitude varied depending on position, almost all the points are colored in blue, i.e., generating photocurrent at zero bias voltage. When forward bias is applied, the amount of generated photocurrent decreases. At 0.4 V, some regions are colored in red, which indicates current in the opposite direction, i.e., the leakage current. At 0.6 V, almost half of the surface region generates current and the other half loses current through leakage. This is because the local V_{OC} is above 0.6 V in the former region and is below 0.6 V in the latter region. Interestingly, the lower part of the lower-right yellow elliptical region now starts leaking current even though this part exhibited the highest J_{SC} in Fig. 5(a). At 0.8 V, some portion of the sample still generates a small photocurrent while the leakage current in other parts overcomes this generation. At 1.0 V, almost all the regions are colored in red.
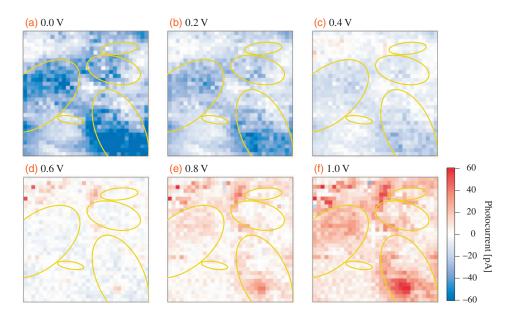

Fig. 5. Sample bias dependence of the photocurrent distribution in the same area as that of Fig. 3. The blue and red colors correspond to photocurrent generation and leakage, respectively.
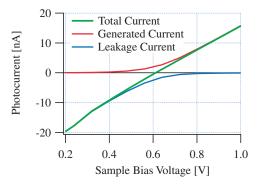
Fig. 6. Total current decomposed into generated and leakage current.

Next, we discuss the macroscopic J–V curve of the device in terms of the observed microscopic J–V curves of the sample. As illustrated in Fig. 1(d), the STM tip collects only a small portion of the generated electrons in the device, whereas the planar metal electrode of an ordinary solar cell device collects all of them, as seen in Fig. 1(c). Thus, we can estimate the total amount of collectable carriers in the device by summing the observed current at different positions. The green curve in Fig. 6 shows the total photocurrent in the whole region observed in Fig. 4 against the bias voltage. This total current is calculated by simply summing the current values measured at each grid point. The generated current (blue) and leakage current (red) are also plotted; these are calculated by summing the current values with negative and positive polarity separately. Here, the negative current corresponds to photocurrent generation. Thus, below 0.61 V, this whole region generates current, whereas, above this bias voltage, leakage current overcomes the generation. At 0.61 V, a photocurrent of 2.2 nA is internally generated, but exactly the same amount of leakage current flows in the other part. Consequently, no current flows out of the device; i.e., this point corresponds to the macroscopic V_{OC}.

Let us now briefly discuss the validity of our observation. Currently, the LM-STS result strongly depends on the individual difference of STM tips. It is known that the generation efficiency of a solar cell depends strongly on the work function of the metal electrode. Improving the reproducibility of LM-STS measurements is currently under investigation by depositing low-work-function materials on the tip apex under UHV. Regarding the "total current", the photocurrent measured by an STM tip flows through a very localized area of <0.1 nm^2 at the tunnel junction. As pointed out in a previous study,[25] however, the current in the sample spreads over a wider area of 10–100 nm depending on the shape of the tip apex and thickness of the film. Thus, the area where the generated carriers are collected from a single grid point overlaps the area where the generated carriers are collected from neighboring grid points. Consequently, the total photocurrent plotted in Fig. 6 is overestimated because of multiple counting of the generated photocurrent. Another concern is the inner resistance. Because the photocurrent measurement by STM forces photocarriers that are generated in 10–100 nm to flow through a very small region beneath the STM tip,

the internal resistance is overestimated in comparison with real devices. This point will be discussed in detail in a future publication. Even with these limitations, this kind of microscopic measurement fortifies our understanding of the determination of macroscopic characteristics of a solar cell from the microscopic view point and will help improve their performances.

In summary, we investigated the microscopic J–V characteristics of a BHJ organic solar cell composed of an MDMO-PPV:PCBM blend by using LM-STS. Elliptic PCBM-rich domains are clearly distinguished by the dark J–V characteristics and they exhibited larger J_{SC} values than the surrounding MDMO-PPV-rich area. When a forward bias voltage is applied, some regions of the sample start leaking the current that is generated in the other regions. The bias voltage at which all the generated current is lost through leakage corresponds to the macroscopic V_{OC}. The macroscopic J–V characteristics can be understood as the generated photocurrent in a part of the device minus the leakage current in other parts of the device.

1) C. W. Tang, Appl. Phys. Lett. **48**, 183 (1986).
2) G. Dennler, M. C. Scharber, and C. J. Brabec, Adv. Mater. **21**, 1323 (2009).
3) T.-Y. Chu, J. Lu, S. Beaupré, Y. Zhang, J.-R. Pouliot, S. Wakim, J. Zhou, M. Leclerc, Z. Li, J. Ding, and Y. Tao, J. Am. Chem. Soc. **133**, 4250 (2011).
4) Y. Sun, C. J. Takacs, S. R. Cowan, J. H. Seo, X. Gong, A. Roy, and A. J. Heeger, Adv. Mater. **23**, 2226 (2011).
5) G. Li, R. Zhu, and Y. Yang, Nat. Photonics **6**, 153 (2012).
6) H. F. Dam and F. C. Krebs, Sol. Energy Mater. Sol. Cells **97**, 191 (2012).
7) L. Dou, J. You, J. Yang, C.-C. Chen, Y. He, S. Murase, T. Moriarty, K. Emery, G. Li, and Y. Yang, Nat. Photonics **6**, 180 (2012).
8) B. Mazhari, Sol. Energy Mater. Sol. Cells **90**, 1021 (2006).
9) C. G. Shuttle, R. Hamilton, B. C. O'Regan, J. Nelson, and J. R. Durrant, Proc. Natl. Acad. Sci. U.S.A. **107**, 16448 (2010).
10) R. C. I. MacKenzie, T. Kirchartz, G. F. A. Dibb, and J. Nelson, J. Phys. Chem. C **115**, 9806 (2011).
11) T. Kirchartz, T. Agostinelli, M. Campoy-Quiles, W. Gong, and J. Nelson, J. Phys. Chem. Lett. **3**, 3470 (2012).
12) P. Kumar and A. Gaur, J. Appl. Phys. **113**, 094505 (2013).
13) T. Martens, J. D'Haen, T. Munters, Z. Beelen, L. Goris, J. Manca, M. D'Olieslaeger, D. Vanderzande, L. De Schepper, and R. Andriessen, Synth. Met. **138**, 243 (2003).
14) A. Alexeev, J. Loos, and M. M. Koetse, Ultramicroscopy **106**, 191 (2006).
15) A. Alexeev and J. Loos, Org. Electron. **9**, 149 (2008).
16) O. Douhéret, A. Swinnen, S. Bertho, I. Haeldermans, J. D'Haen, M. D'Olieslaeger, D. Vanderzande, and J. V. Manca, Prog. Photovoltaics **15**, 713 (2007).
17) D. C. Coffey, O. G. Reid, D. B. Rodovsky, G. P. Bartholomew, and D. S. Ginger, Nano Lett. **7**, 738 (2007).
18) M. Hiramoto, H. Fujiwara, and M. Yokoyama, Appl. Phys. Lett. **58**, 1062 (1991).
19) G. Yu, J. Gao, J. C. Hummelen, F. Wudl, and A. J. Heeger, Science **270**, 1789 (1995).
20) P. Heremans, D. Cheyns, and B. P. Rand, Acc. Chem. Res. **42**, 1740 (2009).
21) O. Takeuchi, S. Yoshida, and H. Shigekawa, Appl. Phys. Lett. **84**, 3645 (2004).
22) S. Yoshida, Y. Kanitani, R. Oshima, Y. Okada, O. Takeuchi, and H. Shigekawa, Phys. Rev. Lett. **98**, 026802 (2007).
23) PEDOT-PSS: poly(3,4-ethylenedioxythiophene)-poly(4-styrenesulfonate).
24) S. Grafström, J. Appl. Phys. **91**, 1717 (2002).
25) O. G. Reid, K. Munechika, and D. S. Ginger, Nano Lett. **8**, 1602 (2008).